

An introduction to quantum-enhanced sensing using nitrogen-vacancy (NV) centers in diamond.

TA: Matt K. Fu (Dabiri Lab)
Lab: Firestone B290 (The Jelly Lab)
Phone: +1.626.817.3579
Office: Firestone 188
mkfu@caltech.edu

December 4, 2022

Abstract

Quantum sensors use quantum systems or phenomena to measure physical quantities of interest, often with sensitivities and spatial resolutions that exceed what is achievable with classical sensors. You will be introduced to the basics of quantum sensing through the use of an emerging sensing platform based on nitrogen-vacancy (NV) centers in diamond. NV centers are point defects within a diamond lattice whose energy states are highly sensitive to external perturbations such as temperature, strain, magnetic fields, and electric fields. Students will learn the physics that govern this sensor and how to optically initialize, manipulate, and read out their energy states to measure the quantities of interest. Students will then demonstrate their knowledge by measuring the magnetic field vectors created by a permanent magnet via optically detected magnetic resonance (ODMR) of the NV centers.

1 Goals of the experiment

The goal of these experiments is to learn the physics and operation of an emerging quantum sensing platform based on Nitrogen-vacancy centers in diamond. While these experiments will focus on magnetometry, the skills and methodology apply equally well to sensing a wide array of parameters. Over the next three weeks, you will learn how to:

1. Optically initialize and read-out the spin state of a Nitrogen-Vacancy center ensemble,
2. Manipulate the spin-state of the Nitrogen-Vacancy centers with microwaves, and
3. Measure magnetic fields with an ensemble of Nitrogen-Vacancy centers via continuous-wave optically detected magnetic resonance.

2 What is a quantum sensor

In colloquial terms, quantum sensing uses *quantum systems*¹ to measure a physical quantity that can be classical or quantum in nature. In contrast to quantum computing applications, which require highly stable quantum systems that are insensitive to unwanted disturbances, quantum sensing applications exploit the inherent sensitivities of quantum systems to precisely measure physical parameters. The promise of this approach is the ability to achieve measurement sensitivities, precision, and resolutions that often exceed what is practically, and sometimes theoretically, achievable with classical sensing approaches. However, the challenge in realizing these advantages are sizeable and stem from the inherent difficulty in preparing,

¹A quantum system has behavior and energy levels that are explicitly governed by the laws of quantum mechanics rather than those of classical physics.

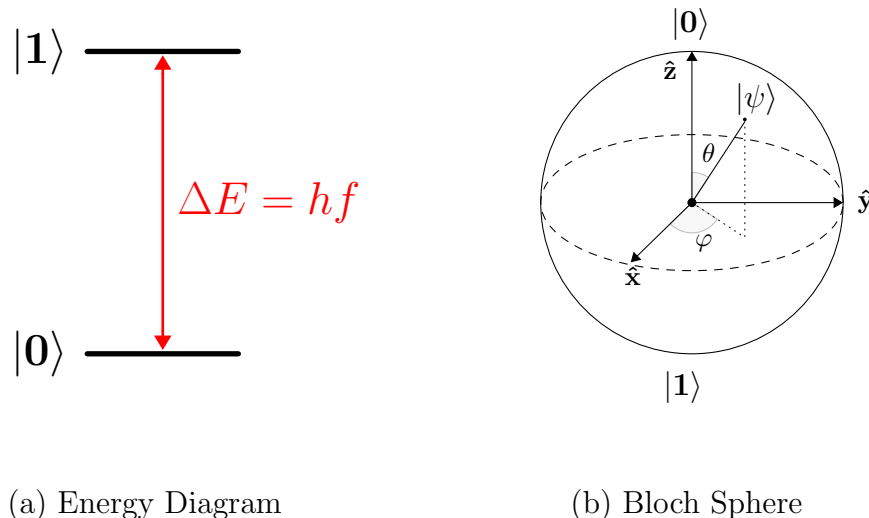


Figure 1: Two diagrams of a two-state quantum system or qubit. Left: Energy diagram showing a lower energy state, $|0\rangle$, and higher energy state $|1\rangle$ separated by an energy $\Delta E = hf$, where h is the Planck's constant. Many forms of quantum sensors have energy differences (ΔE), or rather the state-transition frequencies (f), that change in response to external stimuli. Right: Bloch sphere representation of a two-state qubit. Just as the system on the left, there are two energy states, $|0\rangle$ and $|1\rangle$, but here the antipodal positioning corresponds to these two states being mutually orthogonal states. The pure states of this quantum system ($|\psi\rangle$) correspond to points on the surface of this Bloch sphere, being a linear superposition of our states given by $|\psi\rangle = \cos(\theta/2)|0\rangle + e^{i\varphi}\sin(\theta/2)|1\rangle$.

manipulating, and reading-out these quantum systems. The non-intuitive behavior of quantum systems complicates the ways in which we are allowed to interact with these quantum systems.

Every measurement or experiment, be it classical or quantum, is invasive to some degree. However, in classical systems, we can contrive an “ideal” probe that has a negligible effect on the system we are trying to measure. Consequently, it's possible to faithfully and repeatedly observe our experiment and record the results without worrying that our measurement is influencing the process that we are trying to measure. Most of the examples that you will be considering in Ae 104 fall into this category. For example, flow visualization techniques, such as shadowgraph or Schlieren, can be theoretically be done with almost arbitrarily small amounts of light such that the experiment is unaffected by their momentum and energy. The same is not true, however, for an explicitly quantum system. The act of measuring a quantum system inherently changes something about the system – think Schrödinger's cat.

Before we get much further, let's be a bit more precise about what we mean when we talk about quantum sensors. In their recent review paper, Degen et al. (2017) layout four necessary criteria for a quantum system to function as a quantum sensor

Criteria 1. Quantum system with quantized energy levels: The quantum sensor must have discrete, resolvable energy levels. Examples include many of the quantum systems that are currently being used for quantum computing, such as trapped ions or spin qubits (the latter being what we will be using in this lab). For our purposes, we will treat our quantum sensor as a two-state quantum system, or qubit, with lower energy state, $|0\rangle$, and high energy state, $|1\rangle$. These states will be separated by some transition energy, ΔE , or equivalently, a transition frequency, $f = \Delta E/h$ (see Fig. 1a). Though the quantum system that we will be using in this lab technically has three states, the properties and concepts are well-illustrated by the two-state qubit.

Criteria 2. The transition energy between states is sensitive to external parameters: The quantum system should interact with a relevant physical quantity, V , such that the transition energy changes in response to changes in V . Note, V can be any number of parameters including temperature, voltage, electric fields, strain, pressure, or magnetic fields. Formally, there should exist some sensitivity

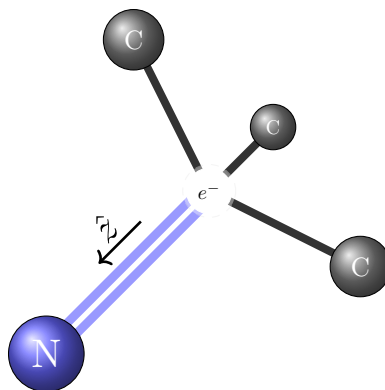


Figure 2: Illustrations of Nitrogen-vacancy center in diamond. Left: Diagram of a single NV center.

parameter $\gamma \equiv \partial^q \Delta E / \partial^q V \neq 0$ that relates the how variation in the transition energy depends on the external parameters with q typically being linear or quadratic (e.g., $q = 1$ or $q = 2$).

Criteria 3. The state can be prepared and read-out: Sensitivity alone is not sufficient for sensing; we must have some means of initializing/preparing the quantum system in a known state and then also reading out the state. A quantum sensor does us no good if we have no way of accessing or interpreting the changes in state. In our system, we will prepare our system in the so-called “ground-state” and manipulate it from there.

Criteria 4. The state can be coherently manipulated: Though not strictly necessary for the technique in this lab, many quantum sensing protocols require that the quantum system can be coherently manipulated.

One last note before delving into our specific quantum system: If we again consider the energy diagram in Fig. 1a, there does not appear to be anything inherently quantum mechanical about this image. In fact, this image appears to equally describe a classical two-state system, i.e., a classical bit. However, we must keep in mind that our quantum system can exist in a superposition of these states, namely some linear combination of states $|0\rangle$ and $|1\rangle$ denoted $|\psi\rangle = \alpha|0\rangle + \beta|1\rangle$, where α and β are complex numbers². Keep in mind that while these coefficients might be imaginary, the fun and probability of quantum systems are all too real! One can show that the space of pure states for $|\psi\rangle$ can be mapped onto the surface of a sphere, called the Bloch sphere, given by $|\psi\rangle = \cos(\theta/2)|0\rangle + e^{i\phi}\sin(\theta/2)|1\rangle$ for angles θ and ϕ . So while our discussion in this lab will pertain to observations of $|0\rangle$ and $|1\rangle$, the state of the quantum sensor will likely involve some superposition of states. This feature is explicitly used for many advanced quantum sensing approaches but is not strictly exploited in this lab.

This might seem quite abstract. In the next section, we will discuss the physics of our quantum system and how it can be employed as a sensor.

3 Nitrogen-vacancy center in diamond as a quantum sensor

The quantum system that you will be working with is a Nitrogen-vacancy (NV) center in diamond. These NV centers are defects within a diamond, i.e., a cubic lattice of elemental carbon, where a vacancy defect is adjacent to a Nitrogen substitution, see Figure 2. Similar to how atomic nuclei are able to bind electrons in surrounding orbitals, the surrounding lattice functions as a solid-state, “inside-out” atom which stabilizes electrons within localized orbitals inside the vacancy. These electrons can stably exist in different quantum states and have gained traction as an accessible, quantum-based method (Degen et al., 2017) for sensing electric and magnetic fields, temperature, strain, and pressure. NV centers have even been proposed as a

²It has recently been demonstrated that these coefficients are indeed complex and not solely real by a recent study in *Nature* by Renou et al. (2021)

method for detecting COVID-19 (Li et al., 2021)!

These sensors, by virtue of being atomic defects, provide the ability to measure the quantities with true nanoscale resolution and proximity. Because they are made of diamond, the NV centers are solid-state quantum devices that are both mechanically robust and biocompatible, and can be chemically functionalized for bio-labeling applications. While the behavior of the NV center becomes easier to predict under cryogenic conditions, the stability of the NV center under a wide range of temperature and pressure conditions, especially atmospheric temperature and pressure, has made it an accessible and attractive option for nanoscale sensing in many applications (Schirhagl et al., 2014). The ability to operate at room temperature is in stark contrast to other quantum sensing devices, such as superconducting quantum interference devices (SQUIDS), which require cryogenic temperatures to operate.

The most common configuration, and the one most useful for sensing, called NV^- , is when six electrons are shared into the vacancy. Three of the electrons are shared from the adjacent Carbon atoms, two are shared from the Nitrogen, and one is donated from the surrounding lattice at large. The six electrons within the vacancy occupy four orbitals whose energy and structure are defined by the C_{3v} symmetry of the NV center. The mechanics of this are complicated and beyond the scope of this lab, but they endow the NV center with some very important properties:

Directionality As can be seen in Fig. 2, there is a natural direction formed by the Nitrogen substitution and vacancy, which is also the axis of symmetry. In a single-crystalline diamond, this axis can be oriented in one of four directions determined by the lattice structure.

Three spin configurations Two of these electrons will be unpaired by the Pauli Exclusion Principle, and their individual spins will either be anti-parallel, resulting in a net spin of zero ($m_s = 0$), or aligned in the up or down direction, corresponding to a net spin of 1 ($m_s = 1$) or -1 ($m_s = -1$), respectively. Remember that m_s is the spin quantum number of the system, with the intrinsic spin of a single electron either $m_s = +1/2$ or $m_s = -1/2$. These three different spin configurations are critical to the operation of the NV center as the energy differences between them are sensitive to a wide array of physical parameters. We will rely on this feature as our quantum sensor to satisfy Criteria 1 and 2. Going forward, we will refer to the three different spin configurations, $m_s = -1, 0$, and 1 as $|-1\rangle$, $|0\rangle$, and $|+1\rangle$, respectively. Note that when we refer to spin, here, we are referring to the quantum of angular momentum inherent to the electrons themselves rather than classical rotation. The resulting angular momentum will have a direction associated within it, but the electrons are not necessarily “spinning”, as such.

Ground and excited energy states Independent of the spin-state of the electrons, the NV center can also exist in either the ground-state, where the electrons occupy the lowest energy orbitals, or an excited-state. The energy difference between these states is associated with optical wavelengths of light. Consequently, the NV center can be elevated into the excited-state with green wavelengths of light and will correspondingly fluoresce red wavelengths of light when returning to ground-state. Where the spin-states will be used for sensing, this feature will be used to initialize and access the state of the NV center sensor, satisfying Criteria 3.

It is important to keep these features in mind for this lab as they will enable the building blocks for our sensing protocols.

4 Optically Detected Magnetic Resonance (ODMR)

In this lab, you will learn one of the simplest methods for using an NV center as a sensor, continuous-wave optically detected magnetic resonance (CW-ODMR). CW ODMR uses the spin-dependent fluorescence of the NV center to determine the energy levels of the different spin states, as shown in Figures 3 and 4. Though this technique can be used to measure nearly all of the quantities to which the NV center is sensitive, you will be using it to measure the magnetic field strength of a permanent magnet.

Consider an NV center initialized in the ground-state. Regardless of the spin, the NV center can be moved from the ground-state into an excited energy state with off-resonant green light (e.g., a 532 nm laser)

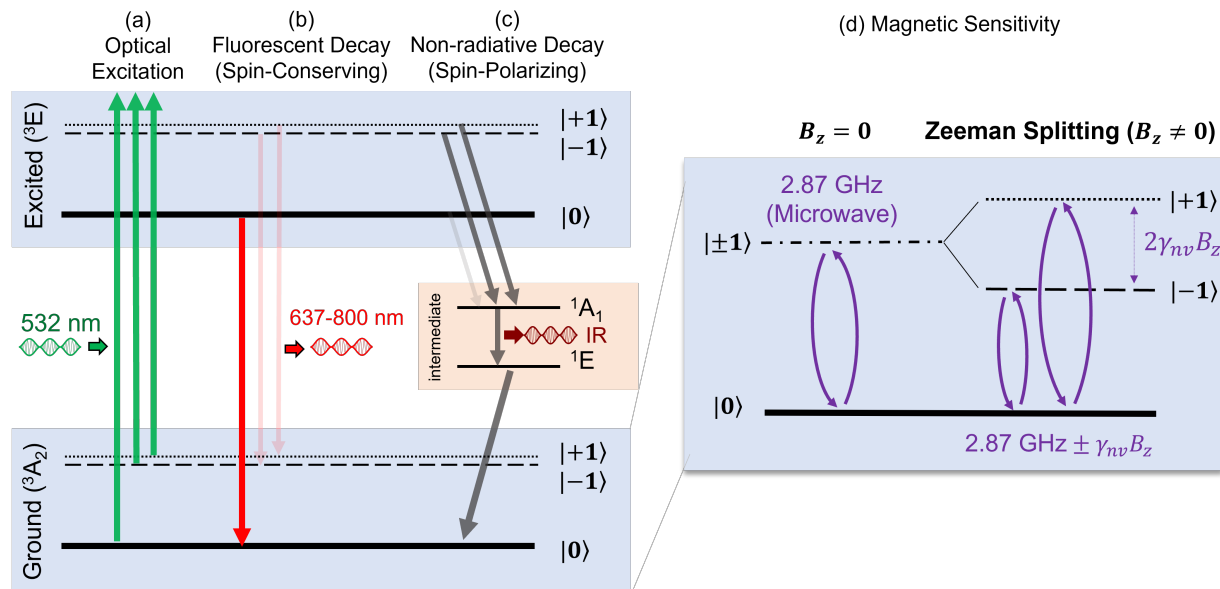


Figure 3: Illustrations of Nitrogen-vacancy center energy levels and transitions. (a) **Spin-preserving optical excitation:** NV centers can be excited from the ground-state (3A_2) to the excited-state (3E). The molecular orbital notations for the ground and excited states are provided in the parentheses. The process of elevating the NV center to the excited energy state preserves the spin-state of the NV center, e.g., NV centers in spin $|0\rangle$ in the ground-state (3A_2) maintain a spin state of $|0\rangle$ in the excited-state (3E). (b) **Spin-conserving Fluorescence:** NV centers in the excited-state (3E) with a spin state of $|0\rangle$ will decay back to the ground-state through a spin conserving pathway. This pathway has an associated fluorescence in the red part of the visual spectrum (600 – 800 nm). (c) **Spin-polarizing, non-radiative decay:** NV centers in the excited-state (3E) with a non-zero spin state ($|\pm 1\rangle$) decay through an intermediate shelving orbital. This pathway has an associated fluorescence in the red part of the visual spectrum (600 – 800 nm). (d) **Spin-state manipulation with microwaves:** The spin-state of the NV center can be manipulated from $|0\rangle \rightarrow |+1\rangle$ and $|0\rangle \rightarrow |-1\rangle$ by microwave pulses. The resonant microwave frequencies that will transition the spin-state depend on a wide variety of physical parameters, including temperature and magnetic fields, as shown in Eq. 1.

without altering the spin configuration of the NV center, see Figure 3(a). However, once in this excited-state, the NV center will decay back down to the ground-state through one of two different paths, depending on its spin number. NV centers with zero spin ($|0\rangle$) will return through the pathway shown in Figure 3(b). This pathway is fluorescent, emitting primarily red wavelengths of light (600 – 800 nm), and also conserves the spin of the NV center (i.e., $|0\rangle$). However, NV centers with non-zero spin numbers ($|\pm 1\rangle$), will instead have a high probability of decaying through the pathway shown in Figure 3(c). In this alternate pathway, the electrons in the NV center pass through several intermediate energy levels, known as singlets energy levels. This pathway is non-optical in that there are primarily non-radiative decay processes with some emission in the infrared spectrum. Consequently, decays through this pathway are distinguished by a *lack* of visible fluorescence.

Did you catch all of that?

To repeat, it is possible to read-out the spin number of the NV center optically! If we shine **green** light on NV centers in spin state $|0\rangle$, they will fluoresce **red** (see Figure 3a-b and Figure 4a). If the NV center is in spin state $|+1\rangle$ or $|-1\rangle$, it will emit **less** red light (see Figure 3a,c, and Figure 4b). Importantly, NV centers decaying through the non-radiative pathway **do not conserve** their spin. The spin number of the NV center is polarized and returned to $|0\rangle$ through an intersystem crossing. This is a non-trivial fact and is necessary for our preparation of the system. Specifically, if our NV center has some non-zero spin state ($|\pm 1\rangle$), it can decay through the non-radiative pathway and be returned to $|0\rangle$. This spin-polarization allows us to *prepare* our system in the ground-state with spin configuration $|0\rangle$ by flooding the system with green light, satisfying the third criteria from Degen et al. (2017).

4.1 Magnetometry

Now that we have a way of reading out the spin-state, we can try to use this feature to measure magnetic fields. Here, we will use the fact that the differences in the spin-state energies are strongly dependent on the strength of the magnetic field at the location of the NV center. These energy differences are strongly influenced by a phenomenon called *Zeeman Splitting*. In the absence of a magnetic field, the energy level of the $|+1\rangle$ and $|-1\rangle$ are degenerate, and transitions from $|0\rangle \rightarrow |\pm 1\rangle$ are resonant with microwaves of frequency $f_{|0\rangle \rightarrow |\pm 1\rangle} = 2.871$ GHz at room temperature (see the left side of Figure 3d). In the presence of a magnetic field with a component aligned with the NV axis, the degeneracy is broken by the *Zeeman Splitting*. The energy of the $|+1\rangle$ state increases relative to the $|0\rangle$, while the energy of the $|-1\rangle$ state decreases. These resonant frequencies can be determined from the spin Hamiltonian of the NV center (see Appendix A) but are most succinctly expressed as

$$f_{|0\rangle \rightarrow |\pm 1\rangle} = D(T) \pm \gamma_{nv} B_z. \quad (1)$$

Here, $f_{|0\rangle \rightarrow |\pm 1\rangle}$ is the resonant microwave frequency to transition the NV center from $|0\rangle \rightarrow |\pm 1\rangle$, $D(T) \approx 2.87$ GHz $- \beta(T - 25^\circ\text{C})$, T is NV center temperature, $\beta = 74$ kHz \cdot K $^{-1}$ (Foy, 2020), B_z is component of the applied magnetic field aligned with the axis of the NV center, and $\gamma_{nv} \approx 28$ GHz \cdot T $^{-1}$. The second term in Eq. 1 captures the effects of the *Zeeman Splitting* on the energy of the $|+1\rangle$ and $|-1\rangle$ states. In the absence of a magnetic field, the two transition frequencies are identical with $f_{|0\rangle \rightarrow |\pm 1\rangle} = D(T)$. However, for a non-zero $|B_z| \neq 0$, there is an energy/frequency difference between the $|+1\rangle$ and $|-1\rangle$ states that is proportional to the field strength of B_z through the scaling factor γ_{nv} (see also the right side of Figure 3d). This frequency difference can be expressed as

$$f_{|0\rangle \rightarrow |+1\rangle} - f_{|0\rangle \rightarrow |-1\rangle} = 2\gamma_{nv} B_z.$$

Thus, if we can calculate the difference between the two transition frequencies, we can determine the strength of the magnetic field component, B_z . Though not part of this lab, Eq. 1 also shows the temperature dependence of the transition frequencies. Where magnetic fields affect the in the cause $f_{|0\rangle \rightarrow |\pm 1\rangle}$ and $f_{|0\rangle \rightarrow |-1\rangle}$, states to diverge, changes in temperature affect these frequencies equally. The frequency shift can

be related to the temperature changes according to the proportionality parameter β as

$$T - 25^\circ = \frac{1}{\beta} \left(\frac{f_{|0\rangle \rightarrow |+1\rangle}}{2} + \frac{f_{|0\rangle \rightarrow |-1\rangle}}{2} - 2.87 \text{ GHz} \right).$$

4.2 Continuous-Wave ODMR

Let's start putting these different aspects together to actually obtain some measurements. Consider a single NV center in the ground-state with spin configuration $|0\rangle$. If we apply microwaves that are far from resonance (i.e., not $f_{|0\rangle \rightarrow |-1\rangle}$ or $f_{|0\rangle \rightarrow |+1\rangle}$) or do not apply any microwaves at all, the NV center will remain in spin configuration $|0\rangle$. Irradiating these NV centers with **green** light will cause the NV center to fluoresce **red**, following the pathway shown in Figure 4a. However, when microwaves are applied to the NV center at or near these resonant frequencies (e.g., $f_{|0\rangle \rightarrow |-1\rangle}$), the spin configuration of the electrons in the NV center will transition out of the $|0\rangle$ state. For example, applying microwaves at $f_{|0\rangle \rightarrow |-1\rangle}$ might transition the NV center out of $|0\rangle$ into the $|-1\rangle$ or, more likely, into some superposition of the $|0\rangle$ and $|-1\rangle$ states. Irradiating these NV centers with **green** light will similarly cause the NV center to enter the excited-state but instead decay back to the ground-state through the “less-radiative” pathway shown in Figure 4b. As the name suggests, the “less-radiative” pathway is distinguished by the absence of red fluorescence observed from the pathway in Figure 4a. CW ODMR uses these two pathways to precisely determine the energy/frequency separation between these different spin states.

In CW ODMR, we apply a continual flux of green light and microwaves (see Figure 5). The frequency of the microwaves is gradually swept over the range of frequencies where we would expect to see the spin state transitions. By monitoring the fluorescence level of the NV center, we can determine the resonant frequencies for the spin transitions, $f_{|0\rangle \rightarrow |-1\rangle}$ and $f_{|0\rangle \rightarrow |+1\rangle}$ as dips in the NV red light emissions. Examples of typical CW ODMR spectra for a single NV center are shown in Figure 4. The fluorescence contrast as a function of applied microwave frequency is shown for three magnetic field strengths, $B_z = 0$ mT, 0.90 mT, and 1.78 mT. Dips in the fluorescence spectra are observed when the frequency of the applied microwaves is resonant with spin transitions from $|0\rangle \rightarrow |\pm 1\rangle$. For $B_z = 0$ mT (top line), only a single dip is observed, indicating the degeneracy of the $|\pm 1\rangle$ states. However, for spectra at $B_z = 0.90$ mT and 1.78 mT (middle and bottom lines, respective), two dips are observed because the degeneracy for the $|-1\rangle$ and $|+1\rangle$ states is broken by the *Zeeman splitting*. The spectral separation between the dips in each case corresponds to $2\gamma_{nv}B_z$. Importantly, the same procedure and logic apply to ensembles of NV centers as it does to individual NV centers.

While the exact shape of the ODMR spectra is setup specific, the shape of contrast dips is well described by a summation of Lorentzian curves or Cauchy distributions given by:

$$C(f; f_n, A_n, \sigma_n) = 1 - \sum_n \frac{A_n \sigma_n^2}{\left[\sigma_n^2 + (f - f_n)^2 \right]}. \quad (2)$$

Here, the ODMR contrast spectrum C is prescribed n Cauchy distributions, each characterized by a central frequency, f_n , peak width σ_n , and maximum contrast A_n . The number of Cauchy distributions (n) is determined as twice the number of NV center orientations in the diamond sample (e.g., eight for a single-crystalline diamond). Similarly, the shot noise limited sensitivity, η_{cw} (Barry et al., 2020) of CW ODMR is given by

$$\eta_{cw} \approx \frac{4}{3\sqrt{3}} \frac{\sigma_n}{\gamma_{nv} A_n \sqrt{\mathcal{R}}} \quad (3)$$

where \mathcal{R} is the photon detection rate. Now that we have the theory, let's look at how we can accomplish this experimentally.

5 Experimental Setup

The microscope system that you will be using is diagrammed in Fig. 6. This microscope delivers green laser light into an ensemble of NV centers and measures their fluorescence through a combination of optical filters and a single-photon counting module. The spin state of the NV centers is manipulated with microwaves to populate our CW ODMR spectra. Details of the equipment are described below.

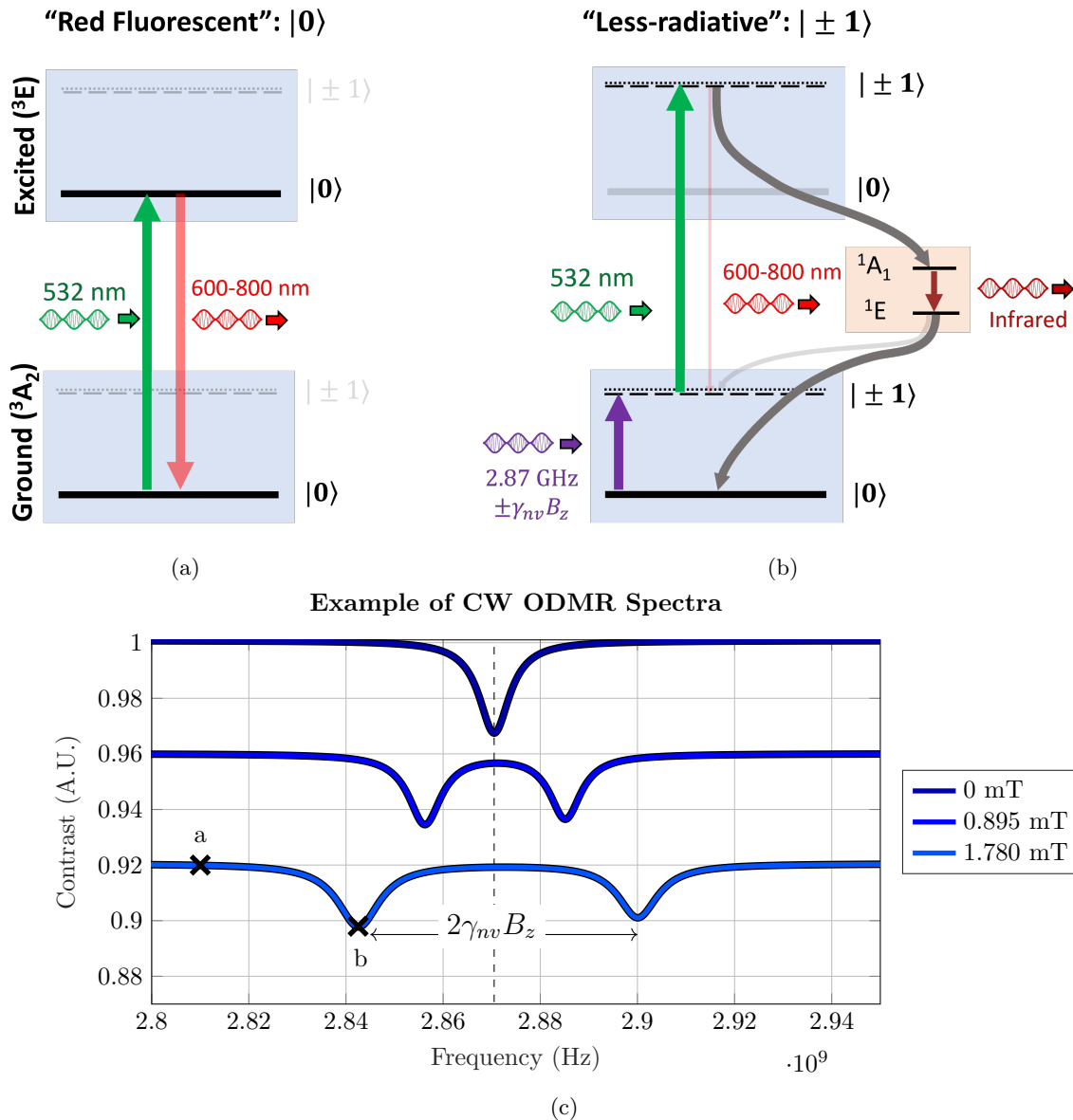


Figure 4: Illustrations of CW ODMR Fluorescence Spectra. **(a) Red-fluorescent pathway:** When no microwaves are applied, or the microwave frequency is not resonant with the spin transition, the NV center will remain in $|0\rangle$. These NV centers will fluoresce red when irradiated with green light. **(b) Less-radiative pathway:** When microwaves are applied at or near the resonant frequency for spin transition, the NV center will transition from $|0\rangle \rightarrow |\pm 1\rangle$. These NV centers will instead partially decay through the intermediate singlet levels after being excited with green light, emitting less red light when returning to the ground-state. The spin configuration of the NV centers upon returning to the ground-state will be polarized to $|0\rangle$. **(c) Typical CW ODMR spectra for single NV center:** Fluorescence contrast for a single NV center as a function of applied microwave frequency under axial magnetic field strengths, $B_z = 0$ mT, 0.90 mT, and 1.78 mT. The spectra are offset by 0.04 from one another for readability. Dips in the spectra indicate the resonant frequency where the NV center transitions from $|0\rangle \rightarrow |\pm 1\rangle$. The contrast spectrum for $B_z = 0$ mT (top line) shows a single dip, indicating the degeneracy of the $|\pm 1\rangle$ states. Contrast spectra for $B_z = 0.90$ mT and 1.78 mT (middle and bottom lines, respective) show two dips where the degeneracy for the $|-1\rangle$ and $|+1\rangle$ states is broken by the *Zeeman splitting*. The spectral separation between the dips in each case corresponds to $2\gamma_{nv}B_z$. (x) : indicate points corresponding to the pathways illustrated in (a) and (b).

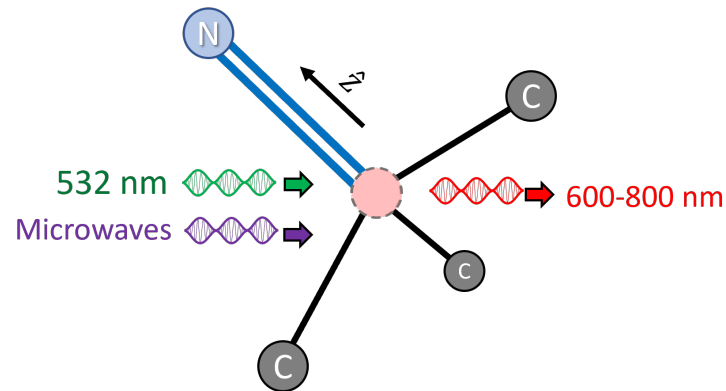


Figure 5: Illustration of CW ODMR. Green light and microwaves of different frequencies are applied to the NV center. The red fluorescence level from the NV center is monitored. The intensity of the fluorescence indicates whether the NV center was in the $|0\rangle$ or a $|\pm 1\rangle$ spin state.

5.1 Optical Microscope

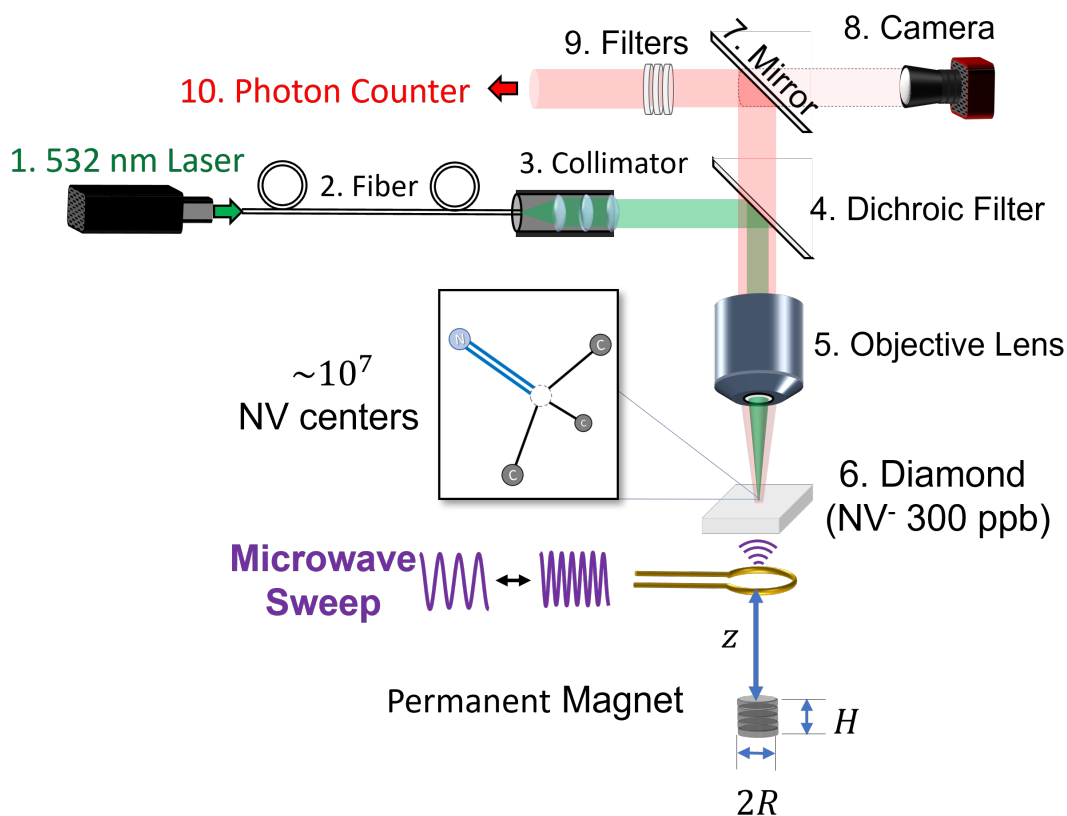


Figure 6: **Illustration of the CW ODMR operation:** Green light (532 nm) is fed into the microscope objective and focused on the diamond sample. The fluorescence from the sample is received by the same objective and filtered to remove the residual excitation light. The spin-states of the NV centers are controlled by microwaves delivered via a ring antenna beneath the sample. See Misonou et al. (2020) for more details.

Preparation and read-out of the NV centers are accomplished optically through the use of a bespoke

microscope system (see Figure 6 for numbering). Optical excitation is provided by the fiber-coupled 200 mW, 532 nm laser (LRS-0532-PFM-00300-03, #1). The laser light is transmitted with a multi-mode fiber optic cable (Laserglow, FC/PC 50 μ m Core, #2) into a triplet collimator (Thorlabs TC18APC-532, #3). The column of light is optionally attenuated with the continuously variable neutral density filter (Thorlabs) and reflected into 100x microscope objective (Olympus LMPLFLN100xBD, NA = 0.8, #5) by a 550 nm cut-on dichroic filter (Thorlabs, DMLP550R, #4). The microscope object fulfills two roles: focusing the green light onto the diamond substrate with microscale resolution (depending on the mode of the fiber) and also collecting the red fluorescence emitted by the diamond sample for read-out. The red fluorescence is received and collimated by the microscope objective and allowed to pass through the dichroic filter, while any residual/reflect green light is reflected back towards the laser source. The imaged light is then passed through a 650 nm long-pass filter (Thorlabs FELH0650) before entering a split cage cube.

At this point, an insertable broadband mirror (Thorlabs BB1-E02, #10) can be used to direct the image light into a CMOS camera (Thorlabs 1.6MP Mono Zelux Camera, #8) for area photoluminescent imaging. In the absence of the mirror, the imaged light passes through a filter stack comprised of a second 650 nm long-pass (Thorlabs FELH0650, #9), 800 short-pass (Thorlabs FESH0800, #9), and a 533 nm notch filter (Thorlabs NF533-17, 17 nm full width at half maximum, #9). The filtered light should retain only the red portion of the visible spectrum corresponding to the NV center emission, as shown in Figure 7. The filtered light passes into an adjustable 10x microscope objective (Newport M-10X), which focused the imaging light onto a multi-mode fiber optic cable (Thorlabs FC/PC 105 μ m Core) and into the single-photon counter module (SPCM, Laser Components, COUNT-10C-FC, #10). Output from the SPCM is in the form of a TTL signal which is monitored by a counter on the DAQ (NI USB-6343). Please refer to Misonou et al. (2020) for additional diagramming and illustrations

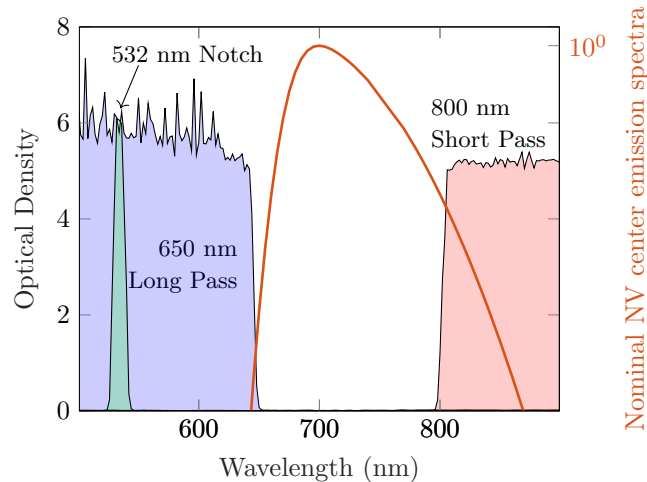


Figure 7: **Optical density of the filter stack as a function of wavelength:** The filtering strength (i.e., optical density) for each component in the filter stack is shown over the visual spectrum. The nominal emission spectrum (log-scaled) for NV^- is shown for reference.

5.2 Microwave Excitation

Microwave excitation is provided by an arbitrary waveform generator (AWG, Anritsu MG3710E) with frequencies between 2.67-3.07 GHz and is used to control the spin state NV centers. The RF signal is sent into the input terminal of an RF switch (Mini-Circuits ZYSWA-2-50DR+, 5 GHz bandwidth), allowing the RF signal to be toggled on and off at frequencies up to 50 MHz. The ability to toggle the microwave with a TTL signal from the DAQ or a function generator is useful for measuring the contrast generated by the microwave excitation and mitigating the effect of laser power drift over time. The first signal output from the switch is connected to a termination impedance, effectively terminating the RF signal when the switch is toggled off. The second signal output terminal from the switch is connected to a 50dB RF amplifier (Mini-Circuits

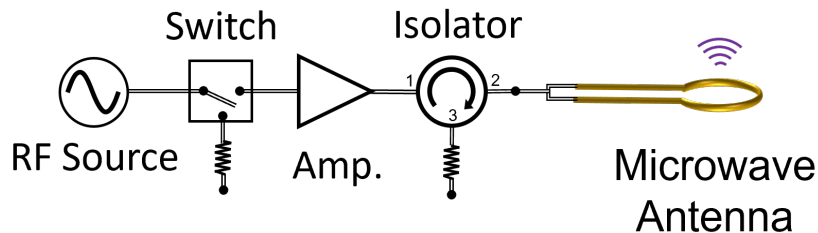


Figure 8: Diagram of the microwave antenna system. The microwaves signal is provided by an arbitrary wave generator (AWG) and toggled on/off by an RF switch. The transmitted signal is amplified by a 50dB amplifier before entering an RF circulator/isolator. The signal from the amplifier is sent into a ring antenna below the NV center sample. Any reflected microwaves are terminated through the last output of the isolator.

ZHL-16W-43+), allowing the RF to pass through when the switch is toggled on. Note, by using the second output of the switch, the RF signal is only connected when a TTL signal is triggered high and is otherwise terminated when the TTL signal is low. The output of the switch is connected to the first connection of an RF circulator functioning as an RF isolator. The second connection of the circulator is connected to the planar ring microwave antenna detailed by Sasaki et al. (2016) and Misonou et al. (2020). Any remaining RF terminals, e.g., the third connection of the circulator, are terminated with impedance matched loads. By putting the circulator/isolator in this configuration, any reflected energy from the antenna will be redirected towards the impedance matched load and dissipated rather than reflected in the amplifier or the AWG. All cables and terminators here are 50Ω impedance.

5.3 MATLAB Connectivity and Control

The data acquisition system has two digital outputs connected to the AWG and the microwave switch. The first triggers the AWG to change the frequency of the RF generator to the next frequency in the microwave sweep. The second toggles the microwave switch, turning the microwave on and off a frequency that exceeds that of the AWG trigger. The DAQ uses three digital inputs. The first two measure the digital outputs to the AWG and microwave to facilitate synchronization of data to the measured frequency and microwave status. The last input is a counter monitoring the TTL signal from the SPCM.

6 Experiments

Part I: CW ODMR Validation and Parameter Selection

Start by removing any magnets from the system and placing the single-crystal diamond beneath the microscope. The objective of this section is to find a set of parameters for the CW ODMR that optimizes the sensitivity of our CW ODMR. Record the fluorescence of the NV center over a 50 MHz bandwidth of microwave frequencies at a 500kHz step size (i.e. 100 points). Toggle the microwave on and off for each frequency set point so you can obtain a fluorescence contrast (i.e., the ratio of the fluorescence with and without microwaves). Vary the laser light and microwave intensities to find the optimal parameters. What microwave and laser powers provide the best shot sensitivity? Consider microwave powers from 10^{-13} W to 0.01 W at five logarithmically spaced points and five laser powers up to 100 mW (approx. 5 on the laser knob).

You should be able to generate *two* plots to convince yourself that the CW ODMR is functioning properly.

1) A map of the estimated shot noise sensitivity as a function of the laser and microwave power and 2) A plot of the phase-averaged fluorescence as a function of microwave phase for the optimum settings at the frequency of peak contrast (i.e., 2.87 GHz).

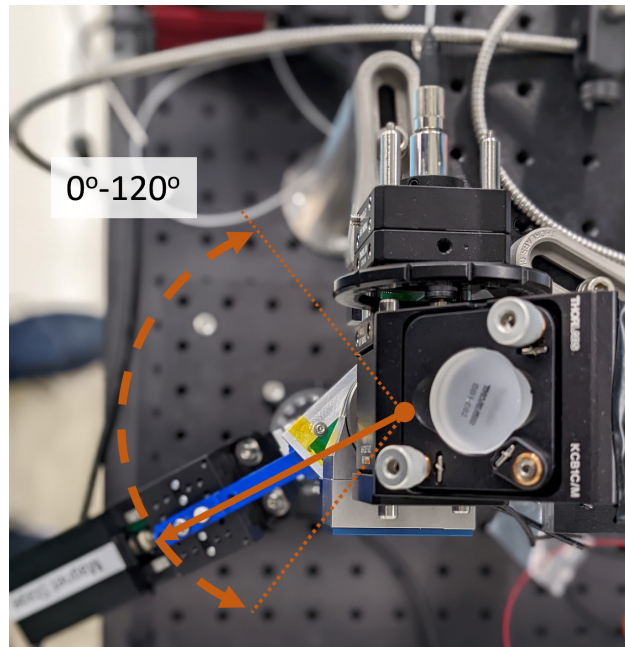


Figure 9: Top-down view of the experimental setup. Rotate the setup at intervals over a range of 120° to identify the orientation that maximizes sensitivity.

Part II: Estimating the magnetic remanence of a permanent magnet

With a suitable set of laser and microwave powers identified, you can now use them to determine the magnetic remanence (i.e., strength) of a cylindrical, permanent magnet. You will do this by measuring the magnetic field strength at different distances (d) along the axis of the magnet and comparing the measurements to the theoretical prediction provided by Blinder (2011) or Misonou et al. (2020) shown in Eq. 4 for a given magnet of radius, R , height h , and remanence B_r . Note that the coordinate system is offset from the top surface of the magnet rather than the center. You will then use these measurements at different distances to estimate the strength of the magnet.

Place the magnet parallel to the surface of the diamond in the horizontal plane. Vary the number of magnets beneath from the diamond and acquire CW ODMR spectra for each. Using an appropriate method of your choosing, identify the spin transition frequencies in the ODMR spectra to estimate the magnetic field strength. Compare the field strength with the theoretical prediction Eq. 4. Now repeat the experiment with the magnet angled at 35.2° from the horizontal plane choosing an azimuthal position (see Figure 9) that maximizes the sensitivity. By symmetry, you won't need to go through all 360 degrees. How many peaks do you see in each configuration, and why? You should be able to generate the following items:

- Plots of the CW ODMR spectra for the single-crystalline NV diamond at the different locations for both the vertical and tilted orientations. Appropriate curve fits should be added if utilized for identifying the “dips”. In the vertical orientation (see Figure 10a) keep the distance fixed but apply 1, 2, and 3 magnets to vary the field strength. In the tilted orientation (see Figure 10b) pick either 2 or 3 magnets, but vary the location of the magnets with the linear actuator.
- Plot the measured magnetic field strength in each case as a function of distance/number of magnets versus the theoretical prediction curve based on your measured magnetic remanence. Do they agree?
- If you have time, you can compare the CW ODMR spectra of the single-crystalline diamond to those found in nanodiamonds (see Matt for details). Which approach is more sensitive and why? Where would one use nanodiamonds instead of the single crystal?

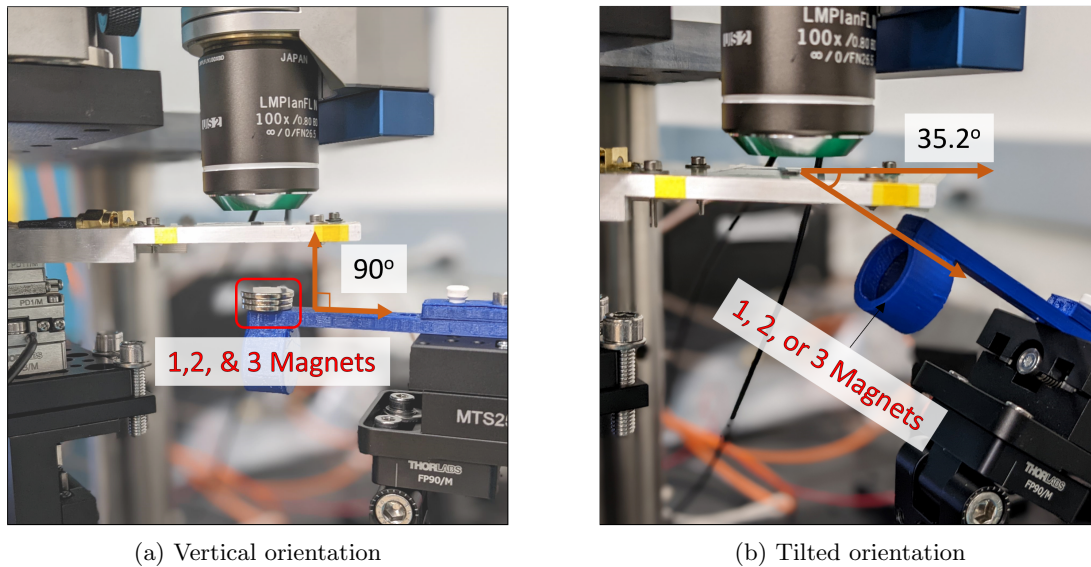


Figure 10: Diagram of the (a) vertical and (b) tilted magnet orientations.

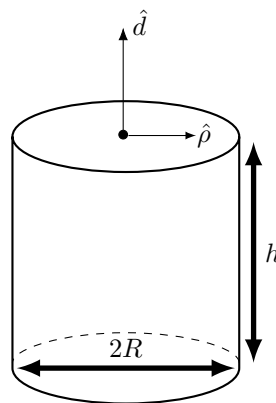


Figure 11: Coordinate system for determining the axial magnetic field strength of a cylindrical magnet where the origin is at the top surface of the magnet. The strength of the axial magnetic field at an axial distance (d) is given in equation 4 for a magnet with radius R , height h , and magnetic remanence, B_r .

$$B_z(d; B_r, R, h, \rho \rightarrow 0) = \frac{B_r}{2} \left(\frac{(h+d)}{\sqrt{(h+d)^2 + R^2}} - \frac{d}{\sqrt{d^2 + R^2}} \right) \quad (4)$$

7 Report Requirements & Outline

Abstract (5 pts)

Provide a succinct (e.g., 150 word) overview of the experiment, results, and conclusions. Enough description so that I can get the gist without reading the whole lab report :)

Introduction (18 pts)

Give an overview of the background, motivation, and theory for the experiment *in your own words*. **Please do not simply plagiarize this document or other resource as this will enrage your otherwise**

friendly neighborhood TA. You want to get the reader up to speed on the *problem* that you are attempting to solve by providing context and background on the state-of-the-field.

- Include some context and background for the state-of-the-art in magnetometry in terms of resolution and sensitivity. (6 pts)
- Provide some motivation for how/why NV centers would be used for different sensing applications. (6 pts)
- Describe just enough of the theory behind the NV center operation and CW ODMR for an uninitiated reader to understand what you are doing and then how it will be used (i.e., the experiments that you will conduct). (6 pts)

Experimental Methodology (22 pts)

Experimental Setup (12 pts)

- Give a brief description of the experimental setup and hardware (6 pts).
- A diagram/schematic (not lifted from the manual :) would be very helpful. (6 pts)

The descriptions should be sufficient to convince a reader that the setup will function correctly, but details such as part numbers are not necessary. The experimental setup should inform *how* you get the NV centers to function as a sensor. I usually prefer PowerPoint[®], but neatly hand-drawn diagrams are acceptable. If you draw your diagrams and plots in Tikz, you will earn my deepest respect and an email of commendation from yours truly, but no extra points.

Procedure & Validation (10 pts)

Describe the procedure and methodology that you followed in the experimental measurements. Include validations and characterizations of the system.

- Sensitivity (i.e., Contrast levels and line widths) as a function of microwave power and laser intensity. Consider microwave powers from 0 dBm to 0.02 dBm at five logarithmically spaced points and five laser powers up to 100 mW (approx. 5 on the laser knob). (4 pts)
- Plot of the fluorescence intensity with the microwave on and off at the chosen laser and microwave intensity (3 pts)
- Characterization of the laser spot size (i.e., photograph of calibration target and laser spot). This will be used to estimate the number of NV centers that are in the ensemble. (3 pts)

Results (30 pts)

Experimentally determine the magnetic remanence of a cylindrical permanent magnet.

- Include plots of the CW ODMR spectra at representative (minimum 3) locations/magnet numbers for both orientations of the magnet. respectively (i.e. vertical and angled). (12 pts)
- Describe how the Zeeman splitting frequencies and magnetic field were estimated. (6 pts)
- Include a plot of the magnetic field measurements obtained from the ODMR as a function of distance in each orientation and how it compares to the theoretical prediction using your experimentally determined remanence. (12 pts)

Discussion (10 pts)

- Discuss the capabilities and limitations of the technique.(4 pts)
- What is the estimated shot noise sensitivity? (2 pts)
- How do your measurements and performance compare with others from the literature? (2 pts)
- Time/space permitting, pontificate on how the sensitivity of magnetometry might differ from between single-crystalline diamonds and randomly oriented nanodiamonds? (1 pt)
- By virtue of the ODMR, you incidentally measured the temperature of the diamond. How does the spatial resolution of your approach compare with other techniques? (1 pt)

Conclusions (5 pts)

How would you propose improving the sensitivity and resolution? Discuss and potential applications where NV center-based sensing could be useful

References & Formatting (10 pts)

Please properly cite and external references and resources that you used in this investigation, including this manual. Include a comprehensive list of references at the end in the style of your choosing. Make sure your figures and tables are properly labelled, legible, and captioned.

Appendices

A Spin-1 Matrices

$$\hat{S} = \begin{pmatrix} \hat{S}_x \\ \hat{S}_y \\ \hat{S}_z \end{pmatrix} \quad (5)$$

with

$$\hat{S}_x = \frac{1}{\sqrt{2}} \begin{pmatrix} 0 & 1 & 0 \\ 1 & 0 & 1 \\ 0 & 1 & 0 \end{pmatrix}, \quad |1, +1\rangle_x = \frac{1}{2} \begin{pmatrix} 1 \\ \sqrt{2} \\ 1 \end{pmatrix}, \quad |1, 0\rangle_x = \frac{1}{\sqrt{2}} \begin{pmatrix} -1 \\ 0 \\ 1 \end{pmatrix}, \quad |1, -1\rangle_x = \frac{1}{2} \begin{pmatrix} 1 \\ -\sqrt{2} \\ 1 \end{pmatrix} \quad (6)$$

$$\hat{S}_y = \frac{i}{\sqrt{2}} \begin{pmatrix} 0 & -1 & 0 \\ 1 & 0 & -1 \\ 0 & 1 & 0 \end{pmatrix}, \quad |1, +1\rangle_y = \frac{1}{2} \begin{pmatrix} -1 \\ -i\sqrt{2} \\ 1 \end{pmatrix}, \quad |1, 0\rangle_y = \frac{1}{\sqrt{2}} \begin{pmatrix} 1 \\ 0 \\ 1 \end{pmatrix}, \quad |1, -1\rangle_y = \frac{1}{2} \begin{pmatrix} -1 \\ i\sqrt{2} \\ 1 \end{pmatrix} \quad (7)$$

$$\hat{S}_z = \begin{pmatrix} 1 & 0 & 0 \\ 0 & 0 & 0 \\ 0 & 0 & -1 \end{pmatrix}, \quad |1, +1\rangle_z = \begin{pmatrix} 1 \\ 0 \\ 0 \end{pmatrix}, \quad |1, 0\rangle_z = \begin{pmatrix} 0 \\ 1 \\ 0 \end{pmatrix}, \quad |1, -1\rangle_z = \begin{pmatrix} 0 \\ 0 \\ 1 \end{pmatrix} \quad (8)$$

B Spin Hamiltonian

$$H/\hbar = \overbrace{D(T) (\hat{S}_z^2)}^{\text{zero-field}} + \overbrace{\gamma_{nv} (\vec{B} \cdot \hat{S})}^{\text{Zeeman Splitting}} + \dots \quad (9)$$

References

- Barry, J.F., Schloss, J.M., Bauch, E., Turner, M.J., Hart, C.A., Pham, L.M., and Walsworth, R.L., “Sensitivity optimization for NV-diamond magnetometry,” Reviews of Modern Physics, Vol. 92, No. 1, 2020, ISSN 15390756.
- Blinder, S.M., “Magnetic Field of a Cylindrical Bar Magnet - Wolfram Demonstrations Project,” 2011.
- Degen, C.L., Reinhard, F., and Cappellaro, P., “Quantum sensing,” Rev. Mod. Phys., Vol. 89, Jul 2017, p. 035002.
- Foy, C.C., Solid-State Spin-Integrated Circuits for Quantum Sensing and Control by, Ph.D. thesis, Massachusetts Institute of Technology, 2020.
- Li, C., Soleyman, R., Kohandel, M., and Cappellaro, P., “SARS-CoV-2 quantum sensor based on nitrogen-vacancy centers in diamond,” Nano Letters, nov 2021, ISSN 1530-6984.
- Misonou, D., Sasaki, K., Ishizu, S., Monnai, Y., Itoh, K.M., and Abe, E., “Construction and operation of a tabletop system for nanoscale magnetometry with single nitrogen-vacancy centers in diamond,” AIP Advances, Vol. 10, No. 2, 2020, ISSN 21583226.
- Renou, M.O., Trillo, D., Weilenmann, M., Le, T.P., Tavakoli, A., Gisin, N., Acín, A., and Navascués, M., “Quantum theory based on real numbers can be experimentally falsified,” Nature, Vol. 600, No. 7890, dec 2021, pp. 625–629, ISSN 1476-4687.
- Sasaki, K., Monnai, Y., Saijo, S., Fujita, R., Watanabe, H., Ishi-Hayase, J., Itoh, K.M., and Abe, E., “Broadband, large-area microwave antenna for optically detected magnetic resonance of nitrogen-vacancy centers in diamond,” Review of Scientific Instruments, Vol. 87, No. 5, may 2016, p. 053904, ISSN 0034-6748.
- Schirhagl, R., Chang, K., Loretz, M., and Degen, C.L., “Nitrogen-vacancy centers in diamond: Nanoscale sensors for physics and biology,” Annual Review of Physical Chemistry, Vol. 65, 2014, pp. 83–105.